Spin-dependent screening and Auger neutralization of He^+ ions in metals

M. Alducin*
Donostia International Physics Center DIPC, P. Manuel de Lardizabal 4, 20018 San Sebastián, Spain

R. Díez Muiño
Centro Mixto CSIC-UPV/EHU, Facultad de Químicas, UPV/EHU, Apartado 1072, 20080 San Sebastián, Spain

J. I. Juaristi
Departamento de Física de Materiales and Centro Mixto CSIC-UPV/EHU, Facultad de Químicas, UPV/EHU, Apartado 1072, 20080 San Sebastián, Spain

(Received 22 January 2004; published 9 July 2004)

The screening of a He^+ ion embedded in a paramagnetic electron gas is studied using density functional theory within the local spin density approximation. We calculate the induced electron density and the induced density of states for each spin orientation, parallel and antiparallel to that of the electron bound to the He^+ ion. Our results show that the screening is preferably due to parallel spin electrons, especially for low electron densities of the medium. In a second step, the rates for Auger neutralization of a He^+ ion in an electron gas are calculated, paying special attention to their dependence on the spin of the electron excited in the Auger process. The results obtained are used to interpret experiments in which the spin polarization of the emitted yield is measured when a He^+ projectile is neutralized in front of a metal surface.

DOI: 10.1103/PhysRevA.70.012901 PACS number(s): 34.50.Dy, 79.20.Rf

I. INTRODUCTION

The study of the screening of a point impurity in an electron gas plays a central role in the characterization of the interaction of probe particles with metal targets. The first approaches to this problem were based on linear response theory, and studied the effect of improving the description of the dielectric function [1,2]. Nevertheless, it was soon realized that a static real charge represents a strong perturbation for the system, and that nonlinear approaches are necessary in order to properly characterize the rearrangement of the electron density it induces [3,4]. In this respect, density functional theory (DFT) has been successfully used in the description of the nonlinear screening of heavy impurities in metals [5–7]. The method consists in solving the self-consistent Kohn-Sham (KS) equations [8,9] for the special case of a static impurity of charge Z_1 embedded in a free electron gas (FEG).

In several studies, the KS orbitals have been used in an approximate way as monoelectronic wave functions. Accordingly, a number of empty orbitals may be fixed in order to mimic impurities with core holes. This approach has been widely and successfully applied to the study of core-electron photoemission [10–12] and calculations of core-hole Auger widths [13]. More recently, similar ideas have been used to incorporate the crystalline nature of the solids using the so-called *ab initio* band structure of the solid to explain detailed features of *KLV* Auger spectra in Si [14]. The problem is that DFT is only strictly valid for the ground state of each symmetry. Hence, within this framework, there is not a theoretical justification to treat the excited state with an empty core hole. Nevertheless, it has been claimed that as much as the core hole can be treated as an external potential, the method should be physically sound [10].

Another important problem treated within this scheme is the interaction of slowly moving ion projectiles in different charge states with solids. In this case, the static approximation is valid for ion velocities below the Fermi velocity of the metal electrons. The strong perturbation induced by the incoming ion is calculated within DFT, as explained above, and its charge state is described by introducing vacancies in the bound KS orbitals. This approach has been used to study the neutralization of the incoming ion via Auger processes [15–17], the charge state dependence of the energy loss [18–20], and the induced kinetic electron emission [21] in the interaction of multicharged ions with metals.

In this work, we present a detailed analysis of the screening of a He^+ ion in a paramagnetic electron gas. Since the He^+ ion constitutes a spin-polarized object, special attention will be paid to the fact of how this affects the screening characteristic, or in other words, what the degree of spin polarization of the induced density screening cloud is. As an application, we also study the Auger neutralization process and how the value of the Auger rates depends on the spin of the excited Auger electron. This study is relevant in connection with recent experimental results in which a strong spin polarization of the emitted electrons is measured when slow He^+ ions are neutralized in their interaction with paramagnetic metal surfaces [22,23].

The problem of calculating Auger rates for the deexcitation-neutralization of He ions incident on a metal surface has been widely treated in literature [24–33]. These works analyze different aspects of the Auger process for the general case of unpolarized projectiles and nonmagnetic surfaces. In short, we can assert that deep knowledge has been achieved about the value of the rates at large atom-surface

*Electronic mail: wapalocm@sq.ehu.es

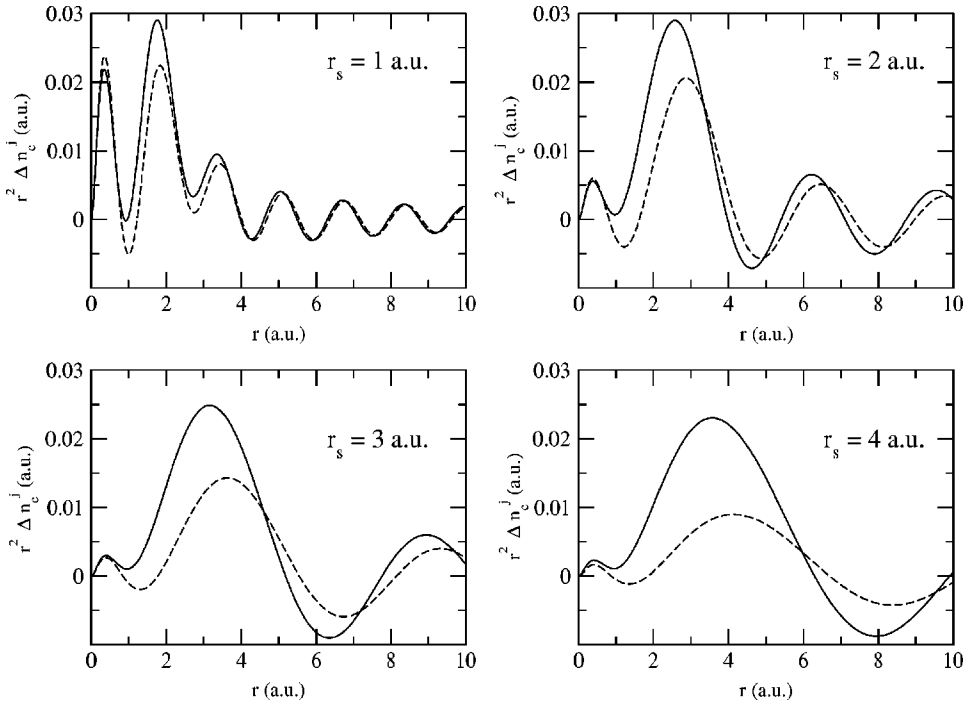

FIG. 1. Radial electron density $r^2\Delta n_c^j(r)$ induced in the continuum by a He^+ ion embedded in a FEG. The electron density of the FEG is indicated in each panel. The He^+ ion with a spin-up electron is at the origin $r=0$. The induced density with spin parallel to the bound electron $\Delta n_c^{\uparrow}$ is shown by solid lines, and that with spin antiparallel $\Delta n_c^{\downarrow}$ by dashed lines.

separations, but that difficulties arise at typical physisorption distances, which are the important ones in the experiments of Refs. [22,23]. A reason for that is the strong perturbation represented by the projectile. This problem was treated in great detail in Ref. [31] for unpolarized projectiles, i.e., without analyzing spin-dependent effects. These effects were partially included in Ref. [34] to study the Auger neutralization of a spin-polarized He^+ ion in front of a Cu surface. The author analyzed the influence in the Auger rate of the exchange process due to the indistinguishability of electrons with identical spin. Nevertheless, the Auger rate was calculated without including the perturbation induced by the ion. In a recent work, the Auger de-excitation of a metastable $2\,^3S$ He^* atom in front of a Na surface has been studied [35]. In this case, the spin-dependent perturbation induced in the target was also included and was shown to be an important effect.

The organization of the present work is as follows. In Sec. II we focus on the screening characteristics of He^+ ions in an electron gas. The main features of the model we use are described and results for the spin-dependent induced electron density and the induced density of states are presented for different values of the electron density of the medium. In Sec. III we apply these results to the study of the Auger neutralization process. The value of the neutralization rates is given as a function of the spin of the excited Auger electron. This allows us to deduce a spin polarization of the emitted electron yield. We also discuss our results in connection to experimental findings. In Sec. IV we give the main conclusions of this work.

Atomic units (a.u.) will be used unless otherwise stated.

II. SPIN-DEPENDENT SCREENING

The interaction between a static charged particle and a FEG requires a nonperturbative theoretical description due to the large rearrangement of electronic charge induced by the particle in its vicinity. DFT within the local density approximation (LDA) has proven to be successful in the calculation of such a displacement of electronic charge [6,7]. For spin-dependent properties, the local spin density (LSD) approximation is needed [36]. The LSD approximation includes electronic exchange and correlation effects through approximate functionals, keeping the simplicity of a one-particle equation with a local potential. The starting point are KS equations [9]

$$\left\{-\frac{1}{2}\nabla^2 + v_{\mathrm{eff}}^j(\mathbf{r})\right\}\varphi_i^j(\mathbf{r}) = \varepsilon_i^j\varphi_i^j(\mathbf{r}), \tag{1}$$

where $\varphi_i^j(\mathbf{r})$ and ε_i^j are the KS wave functions and eigenvalues, respectively. The index j runs over the two spin components $\uparrow$ and $\downarrow$. KS equations are used to obtain, in a self-consistent manner, the electron density of the system $n(\mathbf{r})$:

$$n(\mathbf{r}) = \sum_{j=\uparrow,\downarrow}\sum_{i\in occ.} \left|\varphi_i^j(\mathbf{r})\right|^2. \tag{2}$$

The electron density for just spin-up (spin-down) electrons $n^{\uparrow}(\mathbf{r})$ $[n^{\downarrow}(\mathbf{r})]$ can be defined in a similar way by limiting the sum over occupied states to the required spin component.

For the specific case of a static He^+ ion embedded in a paramagnetic FEG, the effective KS potential $v_{\mathrm{eff}}^j(\mathbf{r})$ is composed of three terms, namely,

$$v_{\mathrm{eff}}^j(\mathbf{r}) = -\frac{2}{r} + \int \frac{d\mathbf{r}'[n(\mathbf{r}') - n_0]}{|\mathbf{r}-\mathbf{r}'|} + v_{xc}^j[n(\mathbf{r}),\zeta(\mathbf{r})], \tag{3}$$

where the first term is the external Coulomb potential created by the He core, the second term is the electrostatic potential made by the induced density, and the third term is the exchange-correlation potential, which we calculate using the LSD parametrization of Ref. [36]. The potential

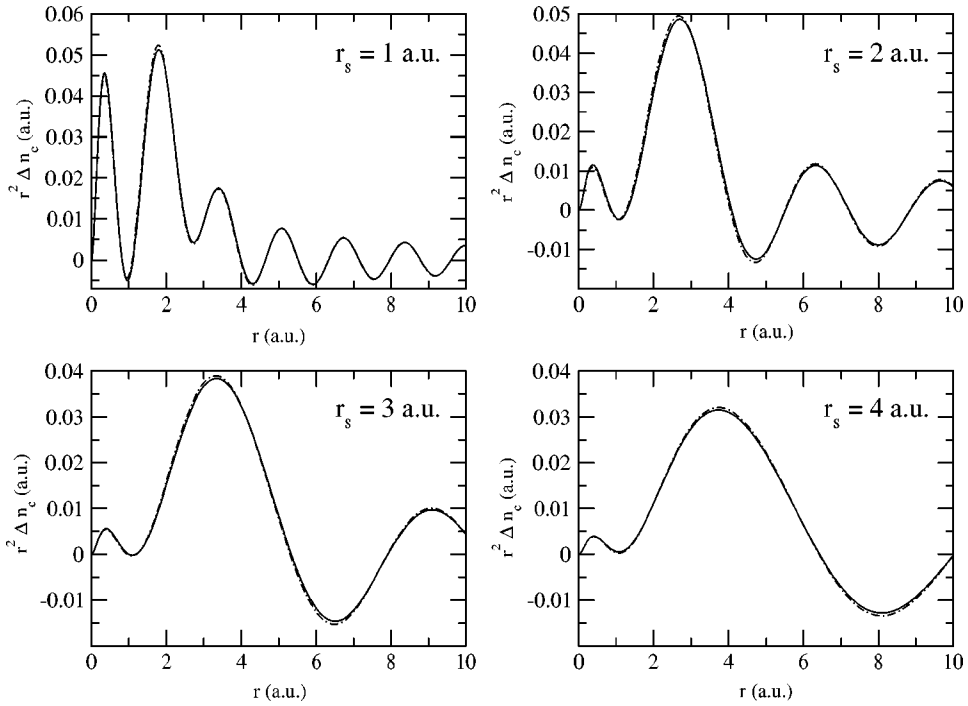

FIG. 2. Total radial electronic density $r^2\Delta n_c(r)$ induced in the continuum by a He^+ ion embedded in a FEG. The electron density of the FEG is indicated in each panel. The He^+ ion with a spin-up electron is at the origin $r=0$. The radial electronic density is calculated using for the exchange-correlation potential the LSD (solid lines) and the LDA (dash-dotted lines) prescriptions.

$v_{xc}^j[n(\mathbf{r}),\zeta(\mathbf{r})]$ is different for each spin component j. It is a function of both the local density $n(\mathbf{r})$ and the local spin polarization $\zeta(\mathbf{r})$, defined as

$$\zeta(\mathbf{r}) = \frac{[n^{\uparrow}(\mathbf{r}) - n^{\downarrow}(\mathbf{r})]}{[n^{\uparrow}(\mathbf{r}) + n^{\downarrow}(\mathbf{r})]}. \tag{4}$$

The electron density of the unperturbed FEG is denoted by n_0, and the customary one-electron radius r_s is defined from $1/n_0=(4/3)\pi r_s^3$.

We follow the same numerical procedure of some other references in the field [7]. The KS wave functions $\varphi_i^j(\mathbf{r})$ are calculated numerically after expansion in the spherical harmonics basis set, and the set of KS equations are solved self-consistently using an iterative procedure. The He^+ ion, in which there is only one bound electron, is modeled by populating just one of the two bound KS 1*s* states of the system (there is one for each spin orientation). In this way, the spin of the electron bound to the projectile is fixed. As a convention, let us denote in the following the spin orientation of the electron bound to the He^+ ion as up ($\uparrow$) orientation. Electron correlation effects make the electronic screening charge $\Delta n^j(\mathbf{r})=n^j(\mathbf{r})-n_0/2$ and the KS effective potential $v_{\mathrm{eff}}^j(\mathbf{r})$ different for each spin orientation. In the latter, this difference is introduced through the spin-dependent exchange-correlation term $v_{xc}^j[n(\mathbf{r}),\zeta(\mathbf{r})]$. Let us remark here that the origin of the FEG local magnetization is the spin-dependent perturbation introduced by the He^+ ion, as the unperturbed FEG is paramagnetic.

The spin-dependent induced electron density $\Delta n^j(\mathbf{r})$ is the sum of two contributions: that of the continuum KS states $\Delta n_c^j(\mathbf{r})$ plus that of the bound KS states $\Delta n_b^j(\mathbf{r})$, if any. In our case, $\Delta n_c(\mathbf{r})=\Delta n_c^{\uparrow}(\mathbf{r})+\Delta n_c^{\downarrow}(\mathbf{r})$ integrates to a unit charge, providing total screening for the He^+ ion.

Figure 1 shows the radial electronic density induced in the continuum $r^2\Delta n_c^j(r)$ by the spin-polarized He^+ ion embedded in a paramagnetic FEG. Different panels correspond to different metal-electron densities, $r_s=1-4$ a.u. The He^+ ion with a spin-up bound electron in its 1*s* state is at the origin, $r=0$. In order to illustrate the effect of the spin-dependent perturbation in the medium, we distinguish between the induced electron density with spin parallel [$\Delta n_c^{\uparrow}(r)$, by solid lines], and antiparallel [$\Delta n_c^{\downarrow}(r)$, by dashed lines], to that of the bound electron. Clearly, from this figure, the piling up of electrons around the He^+ ion is a spin-dependent phenomenon, particularly for intermediate and low metallic densities ($r_s\geqslant 2$). We observe that close to the bound electron, the screening is preferable due to electrons of parallel spin [$\Delta n_c^{\uparrow}(r)$]. This behavior is simply a manifestation of the Coulomb interaction and the Pauli principle; in other words, of *exchange*. Since the 1*s* state and the continuum states are well separated in energy and space, we focus on the effective electron-electron interaction to explain this effect. Thinking in terms of the mean-field formalism, one can treat short-range electron correlations by introducing local-field corrections to the bare Coulomb interaction between electrons. In a paramagnetic FEG, these local-field corrections depend only on the relative spin of electrons. Therefore, one should distinguish between two different kinds of effective electron-electron interactions: $V_{\uparrow\uparrow}$, the interaction between electrons of parallel spin, and $V_{\uparrow\downarrow}$, the interaction between electrons of opposite spin. For parallel spin electrons, both the Pauli principle and Coulomb correlations contribute to the creation of an exchange-correlation hole, reducing the effectiveness of the short-range part of the Coulomb interaction. For antiparallel spin electrons, however, only Coulomb correlations contribute to the creation of the hole, and therefore, the interaction is not so much reduced. As a result, the exchange is typically characterized by

a weaker repulsive interaction between electrons of parallel spin, i.e., $0<V_{\uparrow\uparrow}<V_{\uparrow\downarrow}$. This allows us to understand the effect observed in Fig. 1. In DFT, the correction to the bare Coulomb interaction is incorporated by the $v_{xc}^{j}(\mathbf{r})$ potential. In this respect, Gunnarsson *et al.* already showed the validity of the LSD to reproduce the Hund's first rule for an open-shell atom [36]. For instance, in case of a metastable He^{*} atom this means that the lowest excited state is the triplet $2\ ^3S$ instead of the singlet $2\ ^1S$. Here, our results indicate that the metal electrons participating in the screening of the spin-polarized He^{+} ion also follow a kind of Hund's first rule that favors the alignment of electron spins, provided the Pauli principle is not violated.

In order to get a deeper insight on the screening process, we have also estimated the integrated induced density for each spin direction ($j=\uparrow,\downarrow$),

$$Q_c^j = 4\pi \int_0^\infty dr\, r^2 \Delta n_c^j(r). \tag{5}$$

Note that $Q_c^{\uparrow}+Q_c^{\downarrow}=1$. The ratio $Q_c^{\uparrow}/Q_c^{\downarrow}$ strongly depends on the FEG density. At high densities, e.g., $r_s=1$, the screening is almost equally shared by the spin-up and spin-down electrons. As the FEG density decreases, the contribution of $Q_c^{\uparrow}$ to the charge balance increases. Thus, for $r_s=5$, the screening is practically due to $Q_c^{\uparrow}$ [37].

This behavior is a consequence of the dependence of the exchange-correlation energy on the FEG density [38]. At high metallic densities, exchange-correlation effects are small because the contribution of the kinetic term to the total energy of the system dominates over the interaction terms. As the electron density decreases, the potential energy becomes comparable to the kinetic one, and the exchange effects that favor the alignment of electron spins are important. As a result, we observe that the alignment is stronger for lower FEG densities, provided we are in the range of metallic densities ($1.5\leqslant r_s\leqslant 6$).

Now, let us verify that the spatial distribution of the total screening charge $[\Delta n_c(r)]$ is practically unaffected by the spin-dependent response of the medium. To do so, we also calculate the electron density induced by the He^{+} ion using the non-spin-dependent LDA. The difference between the LSD and the LDA prescriptions is based on the way the exchange-correlation potential v_{xc} is calculated. The LSD assumes that v_{xc} is a function not only of the local charge density but also of the local spin polarization. On the contrary, in the LDA only the local charge density affects the exchange-correlation potential and, as a consequence, one gets $\Delta n_c^{\uparrow}(r)=\Delta n_c^{\downarrow}(r)$. In Fig. 2, we plot the total radial electronic densities induced in the continuum, i.e., $\Delta n_c(r)=\Delta n_c^{\uparrow}(r)+\Delta n_c^{\downarrow}(r)$, according to the LSD (solid lines) and to the LDA (dash-dotted lines) prescriptions. A comparative analysis of these results indicates that, regarding the spatial distribution of induced charge, the He^{+} ion is equally screened in a paramagnetic FEG whether or not the spin polarization of its bound electron is taken into account.

Up to now, we have analyzed the spatial distribution of the metallic electrons accounting for the screening process. Next, we focus on a different quantity, namely, the density of states in momentum space induced by the impurity in the continuum, $\Delta\rho(k)$. The knowledge of $\Delta\rho(k)$ is fundamental in order to understand the properties of the medium since it governs its excitation spectra. For instance, atomic-like resonances induced by ions in the valence band of the FEG can be clearly seen as peaked structures in the $\Delta\rho^j(k)$ function [17]. Here, we calculate the density of states induced in the continuum for each spin state ($j=\uparrow,\downarrow$) as [17,42]

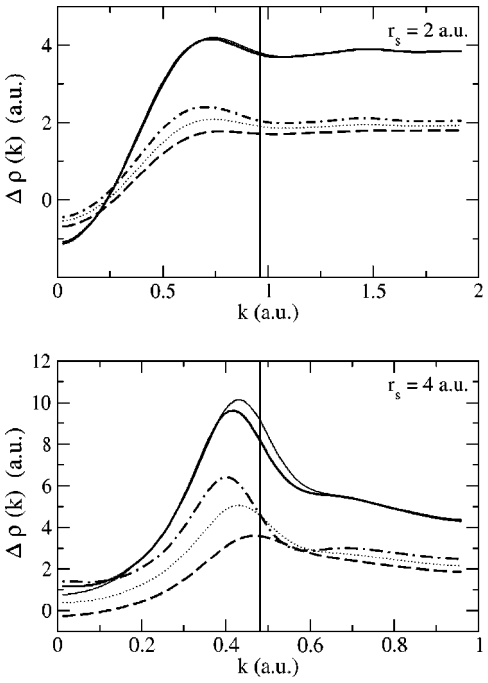

FIG. 3. Density of states $\Delta\rho(k)$ induced in the continuum of a FEG by a He^{+} ion as a function of the electron momentum k. Two different values of r_s are shown: $r_s=2$ (upper panel) and $r_s=4$ (lower panel). The corresponding k_F value is indicated by a vertical line in each panel. Thick lines correspond to the results obtained within the LSD approximation: total $\Delta\rho(k)$ are shown by thick solid lines, $\Delta\rho(k)^{\uparrow}$ by dash-dotted lines, and $\Delta\rho(k)^{\downarrow}$ by long dashed lines. Thin lines represent the results obtained by the LDA prescription: total $\Delta\rho(k)$ (thin solid lines) and partial $\Delta\rho(k)^{\uparrow}=\Delta\rho(k)^{\downarrow}$ (dotted lines).

$$\Delta\rho^j(k) = \frac{2}{\pi}\sum_l (2l+1)\frac{d}{dk}\delta_l^j(k), \tag{6}$$

where k is the electron momentum ($\epsilon=k^2/2$), l is the angular momentum in a partial-wave expansion, and $\delta_l^j(k)$ are the phase shifts of the KS radial wave functions. Figure 3 shows $\Delta\rho^{\uparrow}(k)$ (dash-dotted lines) and $\Delta\rho^{\downarrow}(k)$ (long dashed lines) for two representative metallic densities, $r_s=2$ (upper panel) and $r_s=4$ (lower panel). Thick solid lines correspond to the total density of states, i.e., $\Delta\rho(k)=\Delta\rho^{\uparrow}(k)+\Delta\rho^{\downarrow}(k)$. The value of the Fermi momentum k_F is indicated in each panel by a vertical solid line. For $r_s=2$, the spin-up and -down bands show a quite similar dependence on k. In the region of unoccupied states ($k>k_F$), the difference between $\Delta\rho^{\uparrow}$ and $\Delta\rho^{\downarrow}$ is small and keeps an almost constant value. As is expected, the spin dependence of $\Delta\rho(k)$ is stronger for $r_s=4$. The k

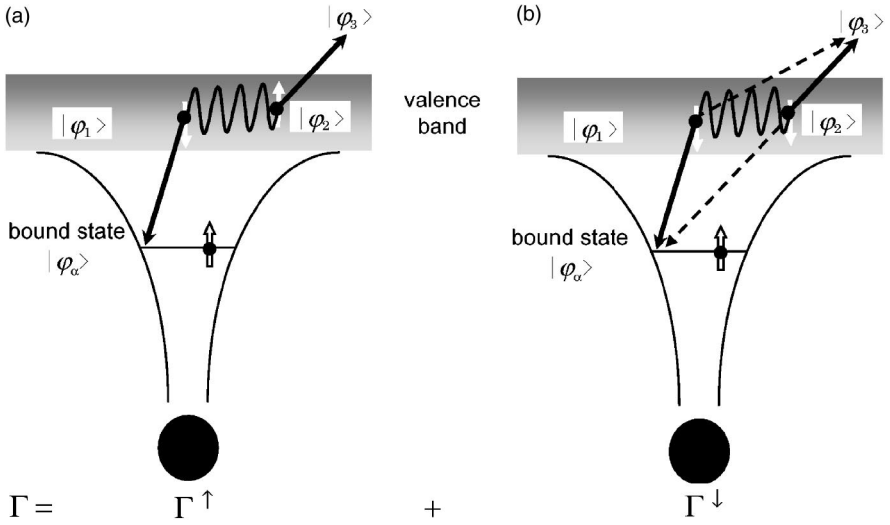

FIG. 4. Schematic representation of the Auger capture process: an electron from the valence band decays to the unoccupied 1*s* state of the He^+ ion, whereas a second electron is excited to an unoccupied continuum state. The Auger process can be viewed as the sum of two channels: (a) $\Gamma^{\downarrow}$, in which the electron excited has a spin parallel to that of the electron bound to the He^+ ion and (b) $\Gamma^{\uparrow}$, in which the spin of the excited electron is antiparallel. The indistinguishability of electrons gives rise in the latter to the two processes indicated by solid and by dashed arrows.

structure of both spin bands are different. $\Delta\rho^{\uparrow}$ shows resonances at $k\sim 0.4$ (below k_F) and $k\sim 0.7$ (above k_F). However, $\Delta\rho^{\downarrow}$ increases smoothly with k and only presents a wide resonance around k_F. Furthermore, the quantitative difference between $\Delta\rho^{\uparrow}$ and $\Delta\rho^{\downarrow}$ is remarkably strong in the region of occupied states, in agreement with the high polarization of the electron density induced around the He^+ ion for this particular value of r_s (see Fig. 1). In the unoccupied region, the difference between both spin bands is smaller.

For the sake of completeness, we also indicate the density of states obtained within the LDA by thin solid lines [total, $\Delta\rho(k)$] and by dotted lines [partial, $\Delta\rho^{\uparrow}(k)=\Delta\rho^{\downarrow}(k)$]. In agreement with the results shown in Fig. 2, at high densities $\Delta\rho(k)$ is unaffected by the spin-polarized nature of the perturbation, even though the screening is not equally shared between both spin bands. For $r_s=4$, however, $\Delta\rho(k)$ is slightly modified, shifting the resonance to lower k values when the local spin polarization is taken into account.

III. AUGER NEUTRALIZATION OF He^+ IONS IN METALS

The embedding of an ion in a FEG is a useful model to describe the interaction between the ion and a metallic medium. In the following, we focus on a specific process involved in this interaction, namely, the Auger capture (AC) process for a He^+ ion in a metal bulk. In a simplified picture, the Auger process is due to the Coulomb interaction between two electrons of the valence band. One electron decays to the empty bound state of the He^+ ion, whereas the second electron is promoted to an excited state. The process is schematically shown in Fig. 4. Two different channels contribute to the total AC probability Γ: (a) capture of a spin-down electron and emission of a spin-up electron $\Gamma^{\uparrow}$ and (b) capture and emission of spin-down electrons $\Gamma^{\downarrow}$.

The AC probability can be calculated in first-order perturbation theory. The probability of AC per unit time involving the excitation of an electron of spin orientation parallel to the bound electron ($\Gamma^{\uparrow}$) is [34,40]

$$\Gamma^{\uparrow}=2\pi\sum_{\varphi_1^{\downarrow}\in occ.}\sum_{\varphi_2^{\uparrow}\in occ.}\sum_{\varphi_3^{\uparrow}\notin occ.}\left|\int d\mathbf{r}\,d\mathbf{r}'[\varphi_\alpha^{\downarrow}(\mathbf{r})]^*[\varphi_3^{\uparrow}(\mathbf{r}')]^* v(\mathbf{r},\mathbf{r}')\varphi_2^{\uparrow}(\mathbf{r}')\varphi_1^{\downarrow}(\mathbf{r})\right|^2\delta(\varepsilon_1^{\downarrow}+\varepsilon_2^{\uparrow}-\varepsilon_\alpha^{\downarrow}-\varepsilon_3^{\uparrow}), \tag{7}$$

where $v(\mathbf{r},\mathbf{r}')=1/|\mathbf{r}-\mathbf{r}'|$ is the Coulomb potential, responsible for the decay. The wave functions of the electrons involved in the transition are approximated by the KS wave functions $\varphi_1^{\downarrow}(\mathbf{r})$ and $\varphi_2^{\uparrow}(\mathbf{r})$ of the He^+/FEG system, with KS eigenvalues $\varepsilon_1^{\downarrow}$ and $\varepsilon_2^{\uparrow}$, respectively. We approximate the wave function of the captured electron in the final state by the KS wave function of the unoccupied bound state $\varphi_\alpha^{\downarrow}(\mathbf{r})$ with eigenvalue $\varepsilon_\alpha^{\downarrow}$. The wave function of the unoccupied state in the continuum is also approximated by the KS wave function $\varphi_3^{\uparrow}(\mathbf{r})$ with eigenvalue $\varepsilon_3^{\uparrow}$.

The Auger probability per unit time when the spin orientation of the excited electron is antiparallel to the bound

electron $\Gamma^{\downarrow}$ needs special care. In this case, the captured electron and the excited electron have the same spin orientation and are thus indistinguishable particles. Hence, the spatial part of the wave function of the two-electron states involved in the transition must be antisymmetric, and $\Gamma^{\downarrow}$ can be written as [34,40]

$$\Gamma^{\downarrow} = 2\pi \sum_{\varphi_1^{\downarrow}\in occ.} \sum_{\varphi_2^{\downarrow}\in occ.} \sum_{\varphi_3^{\downarrow}\notin occ.} \frac{1}{2} \left| \int d\mathbf{r}\, d\mathbf{r}' [\varphi_\alpha^{\downarrow}(\mathbf{r})]^* [\varphi_3^{\downarrow}(\mathbf{r}')]^* v(\mathbf{r},\mathbf{r}') \varphi_2^{\downarrow}(\mathbf{r}') \varphi_1^{\downarrow}(\mathbf{r}) - \int d\mathbf{r}\, d\mathbf{r}' [\varphi_\alpha^{\downarrow}(\mathbf{r})]^* [\varphi_3^{\downarrow}(\mathbf{r}')]^* v(\mathbf{r},\mathbf{r}') \varphi_1^{\downarrow}(\mathbf{r}') \varphi_2^{\downarrow}(\mathbf{r}) \right|^2 \delta(\varepsilon_1^{\downarrow} + \varepsilon_2^{\downarrow} - \varepsilon_\alpha^{\downarrow} - \varepsilon_3^{\downarrow}). \tag{8}$$

The first double integral describes the process indicated in Fig. 4(b) by solid arrows. The last integral corresponds to the indistinguishable process represented by dashed arrows. Expanding the squared term, $\Gamma^{\downarrow}$ can be also written as

$$\Gamma^{\downarrow} = \Gamma_0^{\downarrow} - \Gamma_{int}^{\downarrow} = 2\pi \sum_{\varphi_1^{\downarrow}\in occ.} \sum_{\varphi_2^{\downarrow}\in occ.} \sum_{\varphi_3^{\downarrow}\notin occ.} \left| \int d\mathbf{r}\, d\mathbf{r}' [\varphi_\alpha^{\downarrow}(\mathbf{r})]^* [\varphi_3^{\downarrow}(\mathbf{r}')]^* v(\mathbf{r},\mathbf{r}') \varphi_2^{\downarrow}(\mathbf{r}') \varphi_1^{\downarrow}(\mathbf{r}) \right|^2 \times \delta(\varepsilon_1^{\downarrow} + \varepsilon_2^{\downarrow} - \varepsilon_\alpha^{\downarrow} - \varepsilon_3^{\downarrow}) - 2\pi \sum_{\varphi_1^{\downarrow}\in occ.} \sum_{\varphi_2^{\downarrow}\in occ.} \sum_{\varphi_3^{\downarrow}\notin occ.} \mathrm{Re}\left\{ \int d\mathbf{r}\, d\mathbf{r}' [\varphi_\alpha^{\downarrow}(\mathbf{r})]^* [\varphi_3^{\downarrow}(\mathbf{r}')]^* v(\mathbf{r},\mathbf{r}') \varphi_2^{\downarrow}(\mathbf{r}') \varphi_1^{\downarrow}(\mathbf{r}) \times \int d\mathbf{r}\, d\mathbf{r}'\ \varphi_\alpha^{\downarrow}(\mathbf{r}) \varphi_3^{\downarrow}(\mathbf{r}') v(\mathbf{r},\mathbf{r}') [\varphi_1^{\downarrow}(\mathbf{r}')]^* [\varphi_2^{\downarrow}(\mathbf{r})]^* \delta(\varepsilon_1^{\downarrow} + \varepsilon_2^{\downarrow} - \varepsilon_\alpha^{\downarrow} - \varepsilon_3^{\downarrow}) \right\}, \tag{9}$$

where $\Gamma_0^{\downarrow}$ corresponds to the first term, the one equivalent to the expression of $\Gamma^{\uparrow}$, and $\Gamma_{int}^{\downarrow}$ is the second term preceded by the minus sign.

The indistinguishability of the electrons gives rise to the interference term $\Gamma_{int}^{\downarrow}$, absent in the AC rate $\Gamma^{\uparrow}$. The expression for the AC rate can be also obtained in the self-energy formalism [41]. However, the interference term does not appear in the so-called G^0W^0 derivation at the Hartree level. In this case, one gets [39] $\Gamma_0 = \Gamma^{\uparrow} + \Gamma_0^{\downarrow}$.

The expressions given above for the calculation of the AC probabilities neglect collective effects in the dynamic response of the system to the electron decay. Nevertheless, and for the range of transition energies that are involved in our specific system, these effects should be of minor importance [42]. Further details on the numerical calculation of $\Gamma^{\uparrow}$ and $\Gamma^{\downarrow}$ are provided in the Appendix.

Figure 5 represents the value of the Auger rate as a function of r_s. We show separately the contribution to the total rate coming exclusively from the excitation of electrons with spin-up ($\Gamma^{\uparrow}$, by a thick dash-dotted line) and spin-down ($\Gamma^{\downarrow}$, by a thick dotted line). The total AC rate, $\Gamma = \Gamma^{\uparrow} + \Gamma^{\downarrow}$, is represented by a thick solid line. In this figure, we also show the results obtained without including the interference term: the total rate Γ_0 (thin solid line) and the partial rate $\Gamma_0^{\downarrow}$ (thin dotted line). It is observed that $\Gamma^{\uparrow}$ is much larger than $\Gamma^{\downarrow}$, and that this difference is more important at lower electron densities. The ratio $\Gamma^{\uparrow}/\Gamma^{\downarrow}$ increases a factor of 5 as the electron density varies from $r_s = 2$ to $r_s = 5$.

This difference arises from the contribution of two effects. On the one hand, due to the spin-dependent screening explained in the previous section, it is easier to excite spin-up electrons, because the probability of finding them around the He^+ ion is larger ($\Delta n_c^{\uparrow} > \Delta n_c^{\downarrow}$ close to the ion). The contribution of this effect can be obtained from the comparison of $\Gamma^{\uparrow}$ and $\Gamma_0^{\downarrow}$ (which does not include the interference term). In this case, the difference between the values obtained comes uniquely from the different wave functions entering the matrix elements of $\Gamma^{\uparrow}$ and $\Gamma_0^{\downarrow}$. As can be deduced from the results of the previous section, this effect is important at low electron densities for which the screening is strongly spin dependent. At high densities, the effect is much reduced. On the other hand, a further reduction of the value of $\Gamma^{\downarrow}$ is due to the interference term $\Gamma_{int}^{\downarrow}$, which accounts for the indistinguishability of electrons. A comparison between $\Gamma^{\downarrow}$ and $\Gamma_0^{\downarrow}$ shows that the contribution of this effect to the spin dependence of the AC rate is important over all the range of electronic densities considered. The interference term comes from the fact that the Auger rate is ruled by the Coulomb interaction between electrons, $v(\mathbf{r},\mathbf{r}') = 1/|\mathbf{r}-\mathbf{r}'|$, which is a two-body operator. Therefore, it depends on the two-body density $n(\mathbf{r},\mathbf{r}')$, i.e., the probability of finding a pair of electrons at the positions $\mathbf{r}$ and $\mathbf{r}'$. In $\Gamma^{\downarrow}$, two spin-down electrons participate: the one that is excited and the one that is captured and neutralizes the He^+ ion. Due to the exchange hole that surrounds an electron in the conduction band, the probability of finding two electrons with the same spin close to each other (e.g., the two spin-down electrons in the calculation of $\Gamma^{\downarrow}$) is reduced compared to the case in which the two electrons have different spin. In other words, for small values of $|\mathbf{r}-\mathbf{r}'|$, one has $n_{\downarrow\downarrow}(r,r') < n_{\downarrow\uparrow}(r,r')$. This fact is incorporated in the interference term.

In order to quantify the spin dependence of the Auger process and the influence of the metal electron density on it, we define the spin polarization of the excitation ξ_{AC} by the following expression:

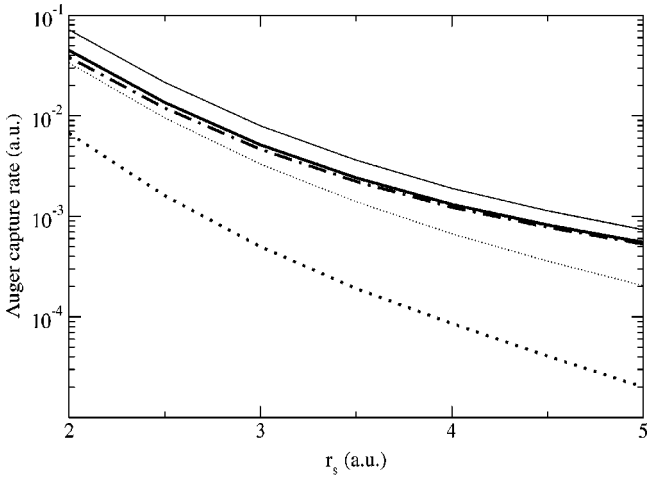

FIG. 5. r_s dependence of the Auger capture rate undergone by a He^+ ion. The thick dash-dotted (thick dotted) line represents the AC rate in which a spin-up (spin-down) electron is excited: $\Gamma^{\uparrow}$ ($\Gamma^{\downarrow}$). The sum of both contributions is shown by a thick solid line. For comparison, we also show the results obtained when the interference term is not included (see text for details). In this case, the total AC rate Γ_0 is indicated by a thin solid line and partial $\Gamma_0^{\downarrow}$ by a thin dotted line.

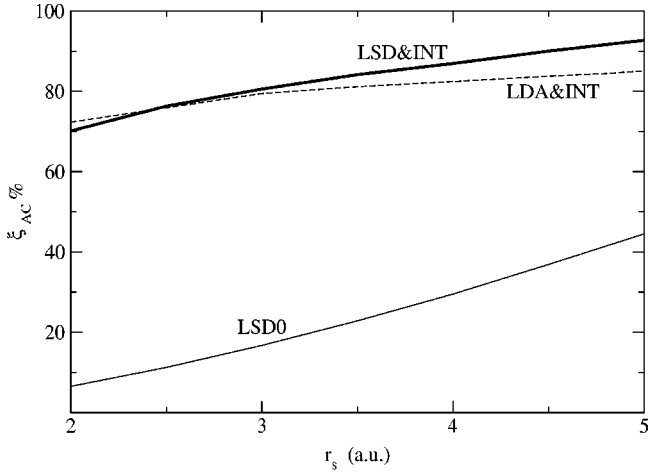

FIG. 6. Spin polarization of the Auger capture rate ξ_{AC}, defined in Eq. (10), as a function of the FEG parameter r_s. The thick solid (dashed) line indicates the results obtained by the LSD (LDA) when the interference term is included. The results obtained by LSD if the latter is not considered are shown by a thin solid line.

$$\xi_{AC} = \frac{\Gamma^{\uparrow} - \Gamma^{\downarrow}}{\Gamma^{\uparrow} + \Gamma^{\downarrow}}. \tag{10}$$

This quantity is related to the average spin polarization of the electrons excited during the Auger capture process. The dependence of ξ_{AC} on r_s is represented in Fig. 6. The curves shown correspond to three different calculations. The thick solid line represents the results obtained using LSD to calculate the screening of the He^+ ion and including the interference term in the calculation of $\Gamma^{\downarrow}$ (we will denote it by LSD&INT). The dashed line is obtained including the interference term but calculating the screening within the LDA (LDA&INT). In this case, the spin dependence of the screening is neglected and all the polarization comes from the interference term. Finally, the thin solid line shows the result of neglecting the interference term in $\Gamma^{\downarrow}$ when the screening is calculated with the LSD prescription (LSD0). Hence, this curve shows the contribution to ξ_{AC} coming exclusively from the spin dependence of the screening. The LSD0 results of the AC rate were already shown in Ref. [39]. Note also that the results obtained in the LSD approximation use the parametrization of Gunnarsson and Lundqvist [36]. We have checked that the use of a different parametrization (Perdew and Wang [43]) introduces differences up to 3% in the spin polarization of the excitation ξ_{AC}. This value can be considered as an estimate of the error introduced by the LSD approximation.

Focusing on the LSD&INT calculation, which incorporates the spin-dependent perturbation induced by the ion and the interference term in $\Gamma^{\downarrow}$, we see that the spin polarization of the excited Auger electrons is very large (70%–90% in the range $r_s=2-5$ a.u.). A comparative analysis of the different curves allows us to deduce the relative importance of these two effects in the spin polarization of the Auger process. By comparing LSD&INT to LSD0, we observe that the interference term plays the predominant role over the entire range of densities. The effect due to the spin-dependent character of the screening (compare LSD&INT to LDA&INT) is always smaller, although it gains relative importance at low densities. Surprisingly, around $r_s=2$, the LSD&INT calculation, which includes the two spin-dependent effects, gives a slightly lower value of ξ_{AC} than the LDA&INT calculation, including only the interference term. The reason is that not only the interference term $\Gamma_{int}^{\downarrow}$, but also $\Gamma_0^{\downarrow}$ and $\Gamma^{\uparrow}$ are modified when using LDA instead of LSD wave functions. Therefore, both the denominator and numerator of Eq. (10) are modified in a nontrivial way. Nevertheless, as one could expect, at low densities for which the screening is strongly spin dependent, the LSD&INT calculation gives the highest value of ξ_{AC}.

In the following, we analyze the polarization of the excited electron as a function of its energy. With this aim, we define the energy-dependent Auger rates $\Gamma^{\uparrow}(\varepsilon_3)$ and $\Gamma^{\downarrow}(\varepsilon_3)$ that are obtained without making the sum over the unoccupied φ_3 states in Eqs. (7) and (9), respectively. In Fig. 7, we show $P(E)$, the polarization of all electrons excited with energies larger than a given value E:

$$P(E) = \frac{\int_E^{E_{max}} d\varepsilon_3 [\Gamma^{\uparrow}(\varepsilon_3) - \Gamma^{\downarrow}(\varepsilon_3)]}{\int_E^{E_{max}} d\varepsilon_3 [\Gamma^{\uparrow}(\varepsilon_3) + \Gamma^{\downarrow}(\varepsilon_3)]}, \tag{11}$$

where E_{max} is the maximum energy for excitation and $E=0$ corresponds to the Fermi level. Note that $P(0)$ is the average polarization ξ_{AC} already shown in Fig. 6. The figure shows that $P(E)$ is an almost constant function with slight variations at the highest values of the energy. For all densities and energies the polarization is very high. The lowest value of $P(E)$ is around 70% for $E=0$ and $r_s=2$.

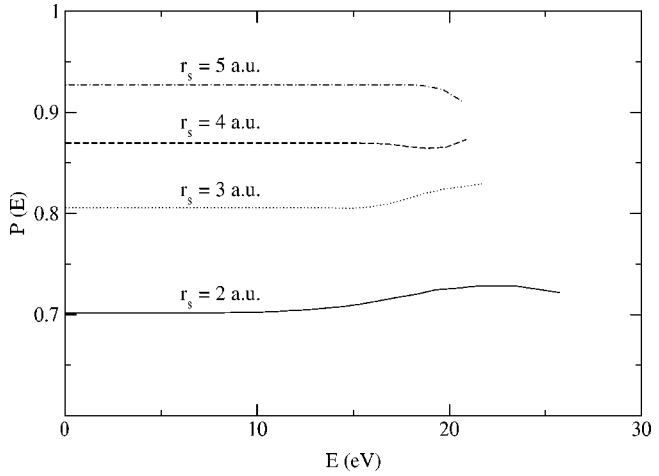

FIG. 7. Spin polarization of all electrons excited with an energy larger than E [see Eq. (11)]. The electron density of the metal is indicated on each curve by the parameter r_s. The energy E is measured from the corresponding Fermi energy E_F.

We would like to remark that the high values we obtain for the polarization of the Auger electrons are consistent with those obtained in similar calculations. In Ref. [34], the polarization of the Auger electrons was calculated for a He^+ ion interacting with a Cu surface. The theoretical model proposed included the interference term, but neglected the perturbation induced by the ion. Similar to our case, the results showed very high values of the polarization (higher than 80%) for the lowest excitation energies. In a recent calculation, Bonini *et al.* [35] obtained the deexcitation rates of a metastable $2\,^3S$ He^* atom interacting with a metal surface, considering both the induced spin-dependent perturbation and the interference term. Although not given explicitly, from their Figs. 5(a) and 5(b), one can infer values of the polarization around 70%.

In Refs. [22,23], the polarization of the emitted Auger electrons when He^+ ions are neutralized in front of different metal surfaces is measured. Although the direction of the measured polarization of the emitted yield coincides with our results (parallel to the spin of the incoming bound electron), there exist quantitative differences. The experiment shows a lower average polarization (around 30%), and only at the highest excitation energies, values of the polarization similar to ours are obtained. Although our work is devoted to a bulk calculation and in the experiment the surface of the metal is probed, this cannot be invoked to explain such a disagreement. One may approximate the Auger rates at a given distance from the surface as the corresponding bulk rates evaluated for the value of the electron density at this position. In this case, to mimic the surface Auger rates, one should use the results we obtain for the lowest values of the density, for which the polarization takes the highest values. Additionally, note that the surface calculations of Refs. [34,35] give values of the polarization close to ours. In Ref. [22], a theoretical model is also presented in order to estimate the values of the polarization of the Auger electrons. In this model, the spin-dependent perturbation induced by an He^+ ion in front of a metal surface was calculated. Assuming that the Auger rates are proportional to the spin-dependent induced electron density of states, they obtain lower values of the polarization than ours, consistent with the measurements. Nevertheless, this model neglects the interference term, or, in other words, assumes that the two-body density is the product of two one-body densities. Note that in the range $r_s=3-4$ a.u. (a reasonable value of the electron density in the surface/vacuum area), our results, without including the interference term, also give around a 30% polarization. Nevertheless, we have shown that to neglect the interference term is too strong an assumption, since it gives an important reduction of $\Gamma^{\downarrow}$.

In connection with the above discussed disagreement between the experimental results and the model calculations, Salmi [34] showed that in order to reproduce the measured lower polarization of the yield, it is necessary to take into account the production of secondary electrons. The excited Auger electrons produce a cascade of nonpolarized secondary electrons mainly in the lower energy region. This effect reduces the polarization at low ejection energies. Note that it is precisely in the low energy region where our calculation overestimates the experimental polarization. Therefore, from our results, we infer that the initial excited Auger electrons are highly spin polarized, and that this polarization is observed experimentally only for high ejection energies. The initial polarization is presumably reduced at low energies due to secondary electrons.

IV. CONCLUSIONS

In this work, we have studied the screening of a spin-polarized He^+ ion in a FEG, using DFT within the LSD approximation. It has been shown that the spin-polarized impurity induces a spin polarization of the medium. The screening is preferably due to electrons with spin parallel to that of the incoming bound electron. The strength of this induced spin polarization of the medium depends strongly on its electron density. In the range of metallic densities, the spin polarization is larger for low electron densities. Whereas for $r_s=1$, the screening is almost equally shared by both kinds of electrons, for $r_s=5$ practically only electrons with parallel spin participate in the screening.

As an application of these results, we have studied the spin polarization of the Auger electrons produced during the neutralization of a He^+ ion in a metal. Our results indicate a large polarization of the Auger rates (larger than 70%), favoring the excitation of parallel spin electrons. The reason for this is twofold: the spin-dependent screening that, close to the He^+ ion, favors the presence of electrons with spin parallel to that of the bound electron; and the interference term of $\Gamma^{\downarrow}$ that incorporates the reduced probability of finding, close to each other, two electrons with the same spin. This last effect is the most important in the entire range of metallic densities. Only at the lowest electron densities does the effect due to the spin-dependent perturbation induced by the ion play an important role in the polarization of the rates. Finally, we point out that our results are consistent with experiments, showing a similar high polarization of the yield for the highest values of the emitted electron energies. Although, for low emitted electron energies, the values of the

measured polarization are lower than those obtained in the model calculations, this is presumably due to the unpolarizing effect of the cascade of secondary electrons, which are emitted with low energies.

ACKNOWLEDGMENTS

We acknowledge partial support by the Basque Departamento de Educación, Universidades e Investigación, the University of the Basque Country UPV/EHU (Grant No. 9/UPV 00206.215-13639/2001) and the Spanish MCyT (Grant Nos. BFM2001-0076 and MAT2001-0946). M.A. acknowledges financial support by the Gipuzkoako Foru Aldundia.

APPENDIX

In this Appendix, we provide some details on the calculation of the Auger rates $\Gamma^{\uparrow}$ and $\Gamma^{\downarrow}$ [see Eqs. (7) and (9)]. Let us start expanding the wave function of the final bound state $\varphi_{\alpha}^{\downarrow}$ in the spherical harmonic basis set

$$\varphi_{\alpha}^{\downarrow} = R_{\alpha l_{\alpha}}^{\downarrow}(r) Y_{l_{\alpha} m_{\alpha}}(\Omega_{\mathbf{r}}), \tag{A1}$$

as well as the wave functions $\varphi_k^j(\mathbf{r})$ of the continuum states with KS eigenvalue $\varepsilon_k^j = k^2/2$:

$$\varphi_k^j(\mathbf{r}) = \sum_{l,m} R_{kl}^j(r) Y_{lm}(\Omega_{\mathbf{r}}) Y_{lm}^*(\Omega_{\mathbf{k}}). \tag{A2}$$

The radial wave functions $R_{kl}^j(r)$ of the continuum states are normalized in such a way that they reduce to the corresponding Bessel functions of the same l in the absence of potential.

The Coulomb potential between the electrons $v(\mathbf{r},\mathbf{r}')$ can be also expanded in terms of spherical harmonics as

$$v(\mathbf{r},\mathbf{r}') = \sum_{l,m} v_l(r,r') Y_{lm}(\Omega_{\mathbf{r}}) Y_{lm}^*(\Omega_{\mathbf{r}'}), \tag{A3}$$

with

$$v_l(r,r') = \frac{4\pi}{(2l+1)} \frac{(r_<)^l}{(r_>)^{l+1}}, \tag{A4}$$

where $r_<$ ($r_>$) is the minimum (maximum) between r and r'.

Introducing the above expansions into Eq. (7), we obtain the following expression for the Auger capture rate $\Gamma^{\uparrow}$:

$$\Gamma^{\uparrow} = \frac{32}{\pi^2} \int_0^{k_F} dk_1 k_1^2 \int_0^{k_F} dk_2 k_2^2 \int_{k_F}^{\infty} dk_3 k_3^2 \sum_{l_1,m_1} \sum_{l_2,m_2} \sum_{l_3,m_3} \left\{ \left| \left[\int \sum_{l,m} dr\, dr'\, r^2 r'^2 [R_{\alpha l_{\alpha}}^{\downarrow}(r)]^* [R_{k_3 l_3}^{\uparrow}(r')]^* v_l(r,r') R_{k_2 l_2}^{\uparrow}(r') R_{k_1 l_1}^{\downarrow}(r) \right.\right.\right.$$
$$\left.\left.\left. \times \int d\Omega_{\mathbf{r}_1} Y_{l_{\alpha} m_{\alpha}}^*(\Omega_{\mathbf{r}}) Y_{lm}(\Omega_{\mathbf{r}}) Y_{l_1 m_1}(\Omega_{\mathbf{r}}) \int d\Omega_{\mathbf{r}'} Y_{l_3 m_3}^*(\Omega_{\mathbf{r}'}) Y_{lm}^*(\Omega_{\mathbf{r}'}) Y_{l_2 m_2}(\Omega_{\mathbf{r}'}) \right] \right|^2 \delta(k_3^2 - (k_1^2 + k_2^2 - 2\varepsilon_{\alpha}^{\downarrow})) \right\}, \tag{A5}$$

where the integrals over the k angles $\Omega_{\mathbf{k}_i}$ have been performed analytically, helping to reduce the number of sums over angular momenta.

The angular integrals over $\Omega_{\mathbf{r}}$ and $\Omega_{\mathbf{r}'}$ can be performed analytically as well, in terms of Wigner $3j$ symbols. After summing over the m indices and making the integral in k_3 by means of the delta function, we obtain the following expression for the Auger rate $\Gamma^{\uparrow}$:

$$\Gamma^{\uparrow} = \frac{16}{\pi^2} \sum_{l,l_1,l_2,l_3} \left\{ \Theta(l_{\alpha},l_1,l_2,l_3;l) \int_0^{k_F} dk_1\, k_1^2 \int_0^{k_F} dk_2\, k_2^2\, k_3^0 |\mathcal{R}^{\uparrow}(l_{\alpha},l_1,l_2,l_3;l)|^2 \right\}, \tag{A6}$$

where we have defined the radial integral $\mathcal{R}^{\uparrow}(l_{\alpha},l_1,l_2,l_3;l)$, which also depends on k_1, k_2, and k_3 as

$$\mathcal{R}^{\uparrow}(l_{\alpha},l_1,l_2,l_3;l) = \int dr\, dr'\, r^2 r'^2 [R_{\alpha l_{\alpha}}^{\downarrow}(r)]^* [R_{k_3 l_3}^{\uparrow}(r')]^* v_l(r,r') R_{k_2 l_2}^{\uparrow}(r') R_{k_1 l_1}^{\downarrow}(r), \tag{A7}$$

the angular coefficient $\Theta(l_{\alpha},l_1,l_2,l_3;l)$ as

$$\Theta(l_{\alpha},l_1,l_2,l_3;l) = \frac{1}{(4\pi)^2} (2l_1+1)(2l_2+1)(2l_3+1)(2l+1) \begin{pmatrix} l_{\alpha} & l & l_1 \\ 0 & 0 & 0 \end{pmatrix}^2 \begin{pmatrix} l_3 & l & l_2 \\ 0 & 0 & 0 \end{pmatrix}^2, \tag{A8}$$

and k_3^0 as $k_3^0 = (k_1^2 + k_2^2 - 2\varepsilon_{\alpha}^{\downarrow})^{1/2}$.

The Auger capture rate when the spin orientation of the emitted electron is antiparallel to the bound electron is made of two terms: $\Gamma^{\downarrow} = \Gamma_0^{\downarrow} - \Gamma_{int}^{\downarrow}$. The first one, $\Gamma_0^{\downarrow}$, is formally identical to $\Gamma^{\uparrow}$, the only difference being the wave functions that must beused in the calculation of the radial integral:

$$\mathcal{R}^{\downarrow}(l_{\alpha},l_1,l_2,l_3;l) = \int dr\, dr'\, r^2 r'^2 [R_{\alpha l_{\alpha}}^{\downarrow}(r)]^* [R_{k_3 l_3}^{\downarrow}(r')]^* v_l(r,r') R_{k_2 l_2}^{\downarrow}(r') R_{k_1 l_1}^{\downarrow}(r). \tag{A9}$$

The interference term $\Gamma_{int}^{\downarrow}$ defined in Eq. (9) can be simplified following a similar procedure. We present here only the final expression

$$\Gamma_{int}^{\downarrow} = \frac{16}{\pi^2} \sum_{l,l',l_1,l_2,l_3} \left\{ \bar{\Theta}(l_\alpha,l_1,l_2,l_3;l,l') \int_0^{k_F} dk_1\, k_1^2 \int_0^{k_F} dk_2\, k_2^2\, k_3^0 \mathcal{R}^{\downarrow}(l_\alpha,l_1,l_2,l_3;l) \mathcal{R}^{\downarrow}(l_\alpha,l_2,l_1,l_3;l') \right\}, \tag{A10}$$

where a sum over an additional index l' is required, and we have defined an angular coefficient $\bar{\Theta}(l_\alpha,l_1,l_2,l_3;l,l')$:

$$\bar{\Theta}(l_\alpha,l_1,l_2,l_3;l,l') = \frac{(-1)^{(l+l')}}{(4\pi)^2}(2l_1+1)(2l_2+1)(2l_3+1)(2l+1)(2l'+1) \begin{Bmatrix} l_1 & l & l_\alpha \\ l_2 & l' & l_3 \end{Bmatrix} \begin{pmatrix} l_1 & l & l_\alpha \\ 0 & 0 & 0 \end{pmatrix} \begin{pmatrix} l_1 & l' & l_3 \\ 0 & 0 & 0 \end{pmatrix} \begin{pmatrix} l_2 & l' & l_\alpha \\ 0 & 0 & 0 \end{pmatrix} \begin{pmatrix} l_2 & l & l_3 \\ 0 & 0 & 0 \end{pmatrix}, \tag{A11}$$

making use of Wigner $3j$ and $6j$ symbols.

[1] J. S. Langer and S. M. Vosko, J. Phys. Chem. Solids **12**, 196 (1960).
[2] K. S. Singwi and M. P. Tosi, Phys. Rev. **181**, 784 (1969).
[3] A. Sjölander and M. J. Stott, Phys. Rev. B **5**, 2109 (1972).
[4] Z. D. Popović and M. J. Stott, Phys. Rev. Lett. **33**, 1164 (1974).
[5] Z. D. Popović, M. J. Stott, J. P. Carbotte, and G. R. Piercy, Phys. Rev. B **13**, 590 (1976).
[6] C.-O. Almbladh, U. von Barth, Z. D. Popović, and M. J. Stott, Phys. Rev. B **14**, 2250 (1976).
[7] E. Zaremba, L. M. Sander, H. B. Shore, and J. H. Rose, J. Phys. F: Met. Phys. **7**, 1763 (1977).
[8] P. Hohenberg and W. Kohn, Phys. Rev. **136**, B864 (1964).
[9] W. Kohn and L. J. Sham, Phys. Rev. **140**, A1133 (1965).
[10] C.-O. Almbladh and U. von Barth, Phys. Rev. B **13**, 3307 (1976).
[11] R. M. Nieminen and M. J. Puska, Phys. Rev. B **25**, 67 (1982).
[12] T. T. Rantala, Phys. Rev. B **28**, 3182 (1983).
[13] C.-O. Almbladh, A. L. Morales, and G. Grossmann, Phys. Rev. B **39**, 3489 (1989).
[14] E. K. Chang and E. L. Shirley, Phys. Rev. B **66**, 035106 (2002).
[15] A. Arnau, P. A. Zeijlmans van Emmichoven, J. I. Juaristi, and E. Zaremba, Nucl. Instrum. Methods Phys. Res. B **100**, 279 (1995).
[16] R. Díez Muiño, N. Stolterfoht, A. Arnau, A. Salin, and P. M. Echenique, Phys. Rev. Lett. **76**, 4636 (1996).
[17] R. Díez Muiño, A. Salin, N. Stolterfoht, A. Arnau, and P. M. Echenique, Phys. Rev. A **57**, 1126 (1998).
[18] J. I. Juaristi and A. Arnau, Nucl. Instrum. Methods Phys. Res. B **115**, 173 (1996).
[19] J. I. Juaristi, A. Arnau, P. M. Echenique, C. Auth, and H. Winter, Phys. Rev. Lett. **82**, 1048 (1999).
[20] J. I. Juaristi, A. Arnau, P. M. Echenique, C. Auth, and H. Winter, Nucl. Instrum. Methods Phys. Res. B **157**, 87 (1999).
[21] J. I. Juaristi, R. Díez Muiño, A. Dubus, and M. Rösler, Phys. Rev. A **68**, 012902 (2003).
[22] D. L. Bixler, J. C. Lancaster, F. J. Kontur, P. Nordlander, G. K. Walters, and F. B. Dunning, Phys. Rev. B **60**, 9082 (1999).
[23] J. C. Lancaster, F. J. Kontur, G. K. Walters, and F. B. Dunning, Phys. Rev. B **67**, 115413 (2003).
[24] H. D. Hagstrum, Phys. Rev. **96**, 336 (1954).
[25] F. M. Propst, Phys. Rev. **129**, 7 (1963).
[26] K. S. Janev and N. N. Nedeljović, J. Phys. B **18**, 915 (1985).
[27] M. Alducin, A. Arnau, and P. M. Echenique, Nucl. Instrum. Methods Phys. Res. B **67**, 157 (1992).
[28] T. Fonden and A. Zwartkruis, Phys. Rev. B **48**, 15603 (1993).
[29] N. Lorente, R. Monreal, and M. Alducin, Phys. Rev. A **49**, 4716 (1994).
[30] M. Alducin, Phys. Rev. A **53**, 4222 (1996).
[31] M. A. Cazalilla, N. Lorente, R. Díez Muiño, J.-P. Gauyacq, D. Teillet-Billy, and P. M. Echenique, Phys. Rev. B **58**, 13991 (1998).
[32] N. P. Wang, E. A. García, R. Monreal, F. Flores, E. C. Goldberg, H. H. Brongersma, and P. Bauer, Phys. Rev. A **64**, 012901 (2001).
[33] E. A. García, N. P. Wang, R. C. Monreal, and E. C. Goldberg, Phys. Rev. B **67**, 205426 (2003).
[34] L. A. Salmi, Phys. Rev. B **46**, 4180 (1992).
[35] N. Bonini, G. P. Brivio, and M. I. Trioni, Phys. Rev. B **68**, 035408 (2003).
[36] O. Gunnarsson and B. I. Lundqvist, Phys. Rev. B **13**, 4274 (1976); **15**, 6006(E) (1977).
[37] As the FEG electron density decreases, the contribution of $Q_c^{\uparrow}$ to the charge screening takes the following values: 57% for $r_s=1$; 61% for $r_s=2$; 66% for $r_s=3$; 75% for $r_s=4$; 90% for $r_s=5$.
[38] P. Nozieres and D. Pines, *The Theory of Quantum Liquids* (Perseus, Cambridge, MA, 1999).
[39] M. Alducin, R. Díez Muiño, J. I. Juaristi, and A. Arnau, J. Electron Spectrosc. Relat. Phenom. (to be published).
[40] P. J. Feibelman, E. J. McGuire, and K. C. Pandey, Phys. Rev. B **15**, 2202 (1977).
[41] P. M. Echenique, J. M. Pitarke, E. V. Chulkov, and A. Rubio, Chem. Phys. **251**, 1 (2000).
[42] R. Díez Muiño, Nucl. Instrum. Methods Phys. Res. B **203**, 8 (2003).
[43] J. P. Perdew and Y. Wang, Phys. Rev. B **45**, 13244 (1992).